# Estimating Significant Wave Height from X-Band Navigation Radar Using Convolutional Neural Networks

**6 authors**, including:

Mikhail Krinitskiy
P.P. Shirshov Institute of Oceanology
**65** PUBLICATIONS **181** CITATIONS

SEE PROFILE

Nikita Anikin
Moscow Institute of Physics and Technology
**8** PUBLICATIONS **7** CITATIONS

SEE PROFILE

Viktor Golikov
Moscow Institute of Physics and Technology
**6** PUBLICATIONS **1** CITATION

SEE PROFILE

Alexander Gavrikov
P.P. Shirshov Institute of Oceanology
**47** PUBLICATIONS **225** CITATIONS

SEE PROFILE

# MACHINE LEARNING
## IN NATURAL SCIENCES

# Estimating Significant Wave Height from X-Band Navigation Radar Using Convolutional Neural Networks

**M. A. Krinitskiy[1, 2, 3]\*, V. A. Golikov[1], N. N. Anikin[1], A. I. Suslov[1], A. V. Gavrikov[1], and N. D. Tilinina[1]**

*[1]Shirshov Institute of Oceanology, Russian Academy of Sciences, Moscow, 117997 Russia*
*[2]Moscow Institute of Physics and Technology, Dolgoprudny, Moscow oblast, 141701 Russia*
*[3]Kazan Federal University, Kazan, 420008 Russia*

**Abstract**—Marine radars are vital for safe navigation at sea, detecting vessels and obstacles. Sea clutter, caused by Bragg scattering, is usually filtered out as noise. It becomes detectable in unfiltered radar images, acquired using SeaVision hardware package, when wind speed and wave height exceed certain thresholds. The parameters of wind-induced ocean waves can be determined using these images; however, traditional spectral methods for obtaining wave characteristics face limitations in improving accuracy. Deep learning techniques offer advantages in image processing tasks, being more robust and able to handle noisier data, yet delivering the results without Fourier transformations and not necessarily requiring long series of radar imagery. In our study, we present the method exploiting convolutional neural networks (CNNs) for estimating wave characteristics from shipborne radar data captured using SeaVision package. In particular, we train our CNN to infer significant wave height using estimates provided by the Spotter buoy as ground truth. Our CNN-based method has an advantage over the classical methods due to the low requirements for radar image data since we process just one SeaVision snapshot, whereas classical method requires more than 20 min of radar images.

## 1. INTRODUCTION

The utilization of marine X-band radars for ship navigation and safety is well-established. However, there is also a significant amount of secondary data that may be extracted from radar digitized images of the sea clutter. In Shirshov Institute of Oceanology of the Russian Academy of Sciences along with Marine Complex Systems Ltd., a hardware package is developed for capturing raw navigation radar data, namely SeaVision (see Fig. 1). In this study, we explore the use of radar images to extract important information about ocean waves, significant wave height (SWH) in particular. The traditional approach for estimating ocean wave parameters using a series of sea clutter images implies three-dimensional Fourier analysis employed to separate signal from background noise. In order to achieve this result, calibration coefficients, attributed specifically to certain

radar models, are used for further determination of ocean wave characteristics; yet, a sequence of radar images of length exceeding 20 min is required for the classical method to deliver SWH estimates. Several commercial and scientific solutions have already implemented these methods for real-time monitoring of wind waves: WaMoS II [1], MIROS [2], SeaDarQ [3], WaveFinder [4], Helmholtz-Zentrum Hereon coherent-on-receive radar [5], and SeaVision [6] (see Fig. 1).

Machine learning techniques have also demonstrated capabilities for the estimation of ocean wave parameters from radar images of the ocean surface. In contrast with the traditional physical-based approach, machine learning potentially makes it possible to overcome the requirements of calibration coefficients, modulation transfer functions and log series of radar images. Recent studies have demonstrated a slightly higher accuracy of artificial neural networks in determining SWH when compared with the tra-
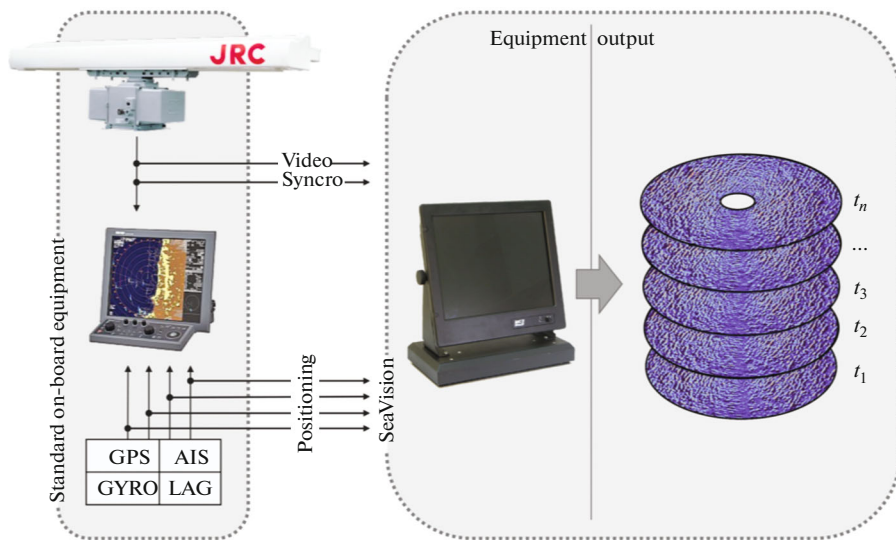
---
*E-mail: `krinitsky@sail.msk.ru`

**Fig. 1.** SeaVision: a hardware package for capturing raw unprocessed radar signal presenting it as individual images representing sea clutter.

ditional Fourier-based approach [7]. Currently, the main limitation in the usage of the neural networks is the requirement for large training subset which should be collected in a wide variety of wave conditions.

As the machine learning (ML) techniques were developing, various models demonstrated their efficiency in radar image processing for estimating ocean waves' characteristics [8−12]. In contrast with abovementioned classical ML models, in recent studies, an approach has been presented of exploiting artificial neural networks in the problem of SWH estimating using radar imagery. In particular, in [7, 8], the authors demonstrated the capabilities of multilayer perceptron (MLP) in estimating wind waves' characteristics on the basis of the data from radars mounted on oil platforms.

The efficacy of convolutional neural networks (CNNs) for pattern recognition in digital imagery has been demonstrated in various applications, including Earth Sciences [13−16]. There are a number of studies demonstrating successful applications of CNNs in estimating wave parameters from marine navigation radar imagery or other types of remote sensing data. For instance, in [17], a CNNs was exploited to estimate real-time SWH based on a series of actual ocean photo images. In [18], a method was presented for processing Sentinel-1 synthetic aperture radar (SAR) images, while in [19], synthetic radar images were used. Hybrid models have also been developed in several recent studies [20−22]. These hybrid models outperform standalone neural networks and classical spectral methods.

In this paper, we present one more algorithm based on machine learning techniques for estimating

SWH from marine shipborne X-band navigation radar equipped with SeaVision capturing package. We redesigned ResNet50 in order to have the capabilities of processing two-dimensional data characterized by a certain periodic structure. Although the approach focuses on a single parameter SWH, it will be extended in the future to other characteristics, such as wave period, wave energy spectra, directional wave spectra, and swell parameters, etc. Compared to other studies, we collected our dataset which includes both SeaVision images of the ocean surface and simultaneous in situ measurements of wave parameters during four research cruises, covering more than 82 locations and containing about 95 000 individual images. The SeaVision hardware package was developed in order to create a vast network of voluntary observing ships using existing marine radars, thus, our goal is to develop a fast yet generalizable algorithm based on ML techniques for estimating wind wave characteristics from marine navigation radar imagery. In this study, we present a low-cost methodology for estimating SWH from SeaVision data along a ship's route, which can overcome the cost constraints of existing systems. The dataset of wave parameters measured by the Spotter buoy and calculated from SeaVision images with spectral methodologies is available at PANGAEA [23] for the first three cruises. Further, we will update the contents of this repository with the new data acquired in upcoming cruises.

The paper is organized further as follows: in Section 2 we provide details of our dataset collected in research cruises; in Section 3, we present the methodology based on convolutional neural networks for estimating SWH from SeaVision imagery; in Section 4,

**Table 1.** Summary of undertaken scientific research marine cruises equipped with SeaVision and Spotter buoy for collecting dataset of this study. Here, abbreviation ASV stands for the research vessel *Akademik Sergey Vavilov*, and AI stands for the research vessel *Akademik Ioffe*

| Mission name | Departure | Arrival | Spotter buoy stations | SeaVision stations |
|---|---|---|---|---|
| ASV50 | Kaliningrad, Russia Aug. 05, 2020 | Arkhangelsk, Russia Sept. 07, 2020 | 24 | 157 |
| AI57 | Kaliningrad, Russia June 29, 2020 | Arkhangelsk, Russia July 11, .2021 | 12 | 76 |
| AI58 | Arkhangelsk, Russia Aug. 04, .2020 | Arkhangelsk, Russia Sept. 05, 2021 | 16 | 55 |
| AI63 | Kaliningrad, Russia Sept. 29, 2022 | Kaliningrad, Russia Dec. 07, 2022 | 30 | 209 |
| **TOTAL** | | | 82 | 497 (6.7 TB) |

we provide the results of our experiments. In concluding Section 5, we summarize the study and highlight its outlook.

## 2. DATA

In this study, we exploy a methodology for collecting data similar to a previous study by Tilinina et al. [6]. Since the paper of 2022, an additional marine research mission has been carried out. Summarized information on the cruises and the map of their routes are presented in Table 1 and Fig. 2. In Table 1, we present the departure and arrival ports along with the number of stations where data from both the Spotter buoy and the SeaVision were collected. Here, a station is an event when the ship is drifting thus providing suitable conditions for the measurements. One may see that the number of Spotter buoy stations differ from SeaVision stations in numbers. That is correct. Since the engineering support for operations at the buoy stations is much more complicated compared to SeaVision operations, some of the SeaVision stations are not supported by buoy measurements. In this study, though, we employ the data of synchronous observations of the Spotter buoy and the SeaVision radar, that are just a subset of the data summarized in Table 1.

In this study, we develop a machine learning model for approximating SWH from SeaVision radar imagery. This ML problem is a supervised regression, thus, one needs to provide a supervision, namely, ground truth values for SWH for each SeaVision radar image. In our study, we employ in situ Spotter wave buoy measurements synchronous to SeaVision radar imagery acquisition. The Spotter buoy is placed in the water away from obstacles and objects disturbing waving conditions; it measures vertical and horizontal displacements of the ocean surface using a set of acceleration and rotation sensors with up to 2.5 Hz sampling frequency [24]. Applying the spectral processing methodology (see details in Tilinina et al. [6]), we retrieve the ground truth for characteristics of wind waves, including SWH.

During the four research cruises of Shirshov Institute of Oceanology of the Russian Academy of Sciences (see Table 1), we collected more than 95 000 SeaVision images and more than 62 h of corresponding Spotter buoy in situ measurements. Both SeaVision and Spotter buoy data are freely available in PANGAEA repository [23].

### 2.1. Data Preprocessing

In this study, we exploit convolutional neural networks (CNNs). CNNs are statistical models characterized by the property of learning the dependences between two-dimensional features and a target variable, namely, SWH. Following the routine procedure, we normalized the target values linearly bringing them to zero mean and unity variance.

At the same time, CNNs are characterized by the sensitivity to noise in source data. ML models are also known for their capability of extracting irrelevant dependences in the case of irrelevant data. During exploratory data analysis of SeaVision radar data, we found that there is a certain pattern in the majority of the images. The most variable signal is observed along the two directions perpendicular to wave ridges (forward and backward w.r.t. waves
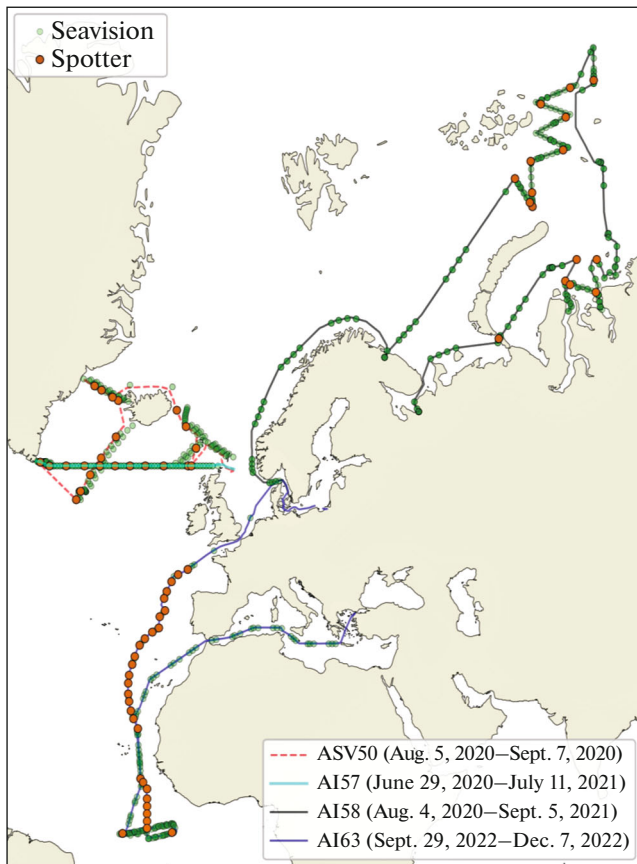
Fig. 2. Map of the routes of our research vessels during the four scientific research marine cruises.
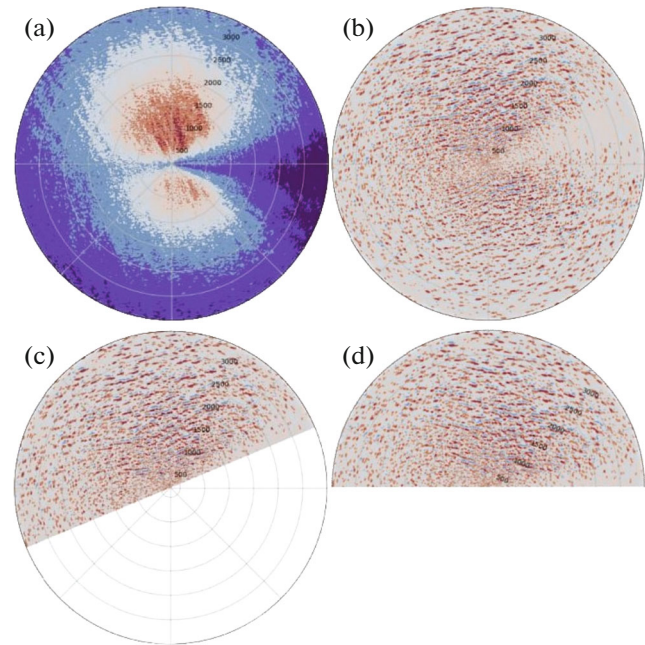


**Fig. 3.** SeaVision data preprocessing scheme: (a) backscattered signal variance computed per pixel through 5-min period; (b) an individual SeaVision radar image; (c) the 180-degree sector that contains maximum median variance; (d) the 180-degree sector of choice in (c) rotated to unified orientaion occupying top semicircle. Here, the variance and radar backscattered data are normalized, thus, we do not present the colorbars. We use colored values here in order to demonstrate the spatial structure of the variance and backscattering magnitude.

propagation direction); yet, along the directions parallel to wave ridges, the variance of the signal and its typical amplitudes are low. Thus, in our study, we preprocess SeaVision images in a manner that preserves relevant spatial features, meaning we select and crop the 180-degree sector containing the most variable signal (see Fig. 3). To do so, we compute the variance of radar backscattered signal in each pixel of the image through the time period of 5 min. Then, we select the 180-degree sector that contains maximum median variance. In Fig. 3, an example of the resulting sector is presented. The values of the variance and SeaVision radar data are normalized to zero mean and unity variance.

CNNs are not inherently rotation invariant, and they require diverse training data with varying spatial features orientation to become rotation invariant. In this study, one may presume that the orientation of the spatial features may not have high diversity of orientations. Thus, we applied two-dimensional data augmentation to source SeaVision radar semicircles including the folowing: random rotation with the angle ranging from $-3°$ to $3°$; random translation with the shift uniformly sampled from the range

$[-5\%, 5\%]$ (meaning percents of image size); scaling with a scale factor uniformly sampled from the range $[0.95, 1.05]$; random left-to-right flip with probability $p = 0.5$. During the augmentation, we also inject additive spatially correlated normal noise of small scale $\sigma = 0.05$. This way, we encourage our CNN to acquire invariance to rotation and translation property through training on augmented data. Applying augmentation, we also enhance generalization ability of our CNN.

In order to retrieve ground truth for SWH, we preprocess Spotter buoy readings in the manner described in detail in Tilinina et al. [6]. In order to unify the methodology, we compute SWH using a fixed time window of 10 min.

## 3. METHODS

In this study, we employ a CNN that we designed for processing SeaVision radar imagery preprocessed in a way described in Subsection 2.1. We constructed the architecture of our CNN following the design of ResNet50 [25]. In contrast with the
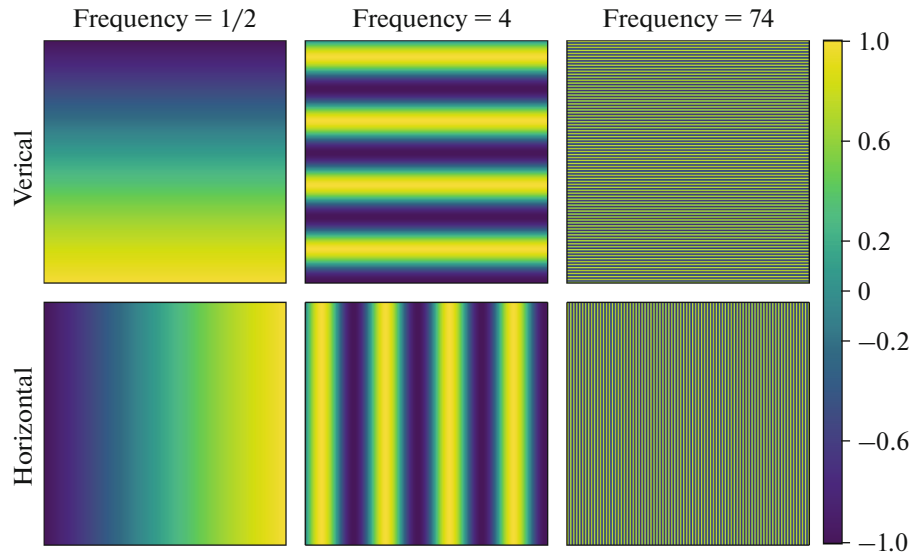
**Fig. 4.** An example of positional encoding maps which we employ in our SinusoidalCoordConv layer in order to inject positional information of spatial features.

original ResNet50, the fully-connected subnet following the convolutional part contains three sequential fully-connected layers of the widths 2048, 512, and 128. The terminating layer is of the width 1 since in this study, we approximate scalar target value SWH. The convolutional part of our modification of ResNet50 is similar to the one described in the original ResNet paper [25] with the reservation of injected sinusoidal positional encoding of various wavelengths. We present this modification of convolutional layer further in Subsection 3.1.

### 3.1. Sinusoidal Positional Encoding

As one may observe from Fig. 3, SeaVision radar images of sea clutter in waving conditions are characterized by some periodic patters with stochastic placement, i.e., the wavelength spectrum of developed wind waves is characterized by distinct modes. One may want a CNN to be capable of capturing these wavelengths using convolutional filters designed by human experts. One more way to explicitly exploit the knowledge of periodic spatial structure of waving sea clutter is to use the Fourier Neural Operator [26]. In our study, we decided to use an alternative inspired by Transformers architecture as well as by the study on the coordinate-injecting convolutional layers [27]. We employ two-dimensional positional encoding which means we inject additional channels of generated harmonic maps characterized by various wavelengths and directions. In particular, we generate the cosine- and sine-based positional encoding channels varying in both horizontal and vertical directions. We concatenate these generated positional encoding maps with activation maps of ResNet building

blocks, thus, the next ResNet block processes activation maps from previous layers along with positional encoding channels. We name these convolutional layers injecting sinusoidal and cosinusoidal positional encoding SinusoidalPositionalEmbedding. In Fig. 4, we present the examples of sinusoidal positional encoding maps which we generate using this module.

In our modification of ResNet50, we do not inject positional encoding maps into conventional ResNet blocks. Instead, we inject it into activation maps of each ResNet building block. In Fig. 5, we present the high-level architecture of our CNN built following this approach.

### 3.2. Training and Evaluation

Artificial neural networks are known to be highly sensitive to the details of the training process, with the choice of training algorithm and hyperparameters being crucial in determining the quality of the resulting model. The Adam algorithm [28] is currently the most stable and widely used training algorithm utilizing a momentum approach to estimate lower-order moments of the loss function gradients. We exploit the Adam optimization procedure in our study.

Of particular importance in optimization algorithms are the batch size and learning rate. Given the large size of SeaVision radar images, we were unable to significantly vary the batch size, and instead opted for the largest batch size that our computer hardware could accommodate (`batch_size=20`) in order to reduce noise in CNN gradient estimates. We also adhered to best practices and optimized the learning rate schedule to achieve not only high quality
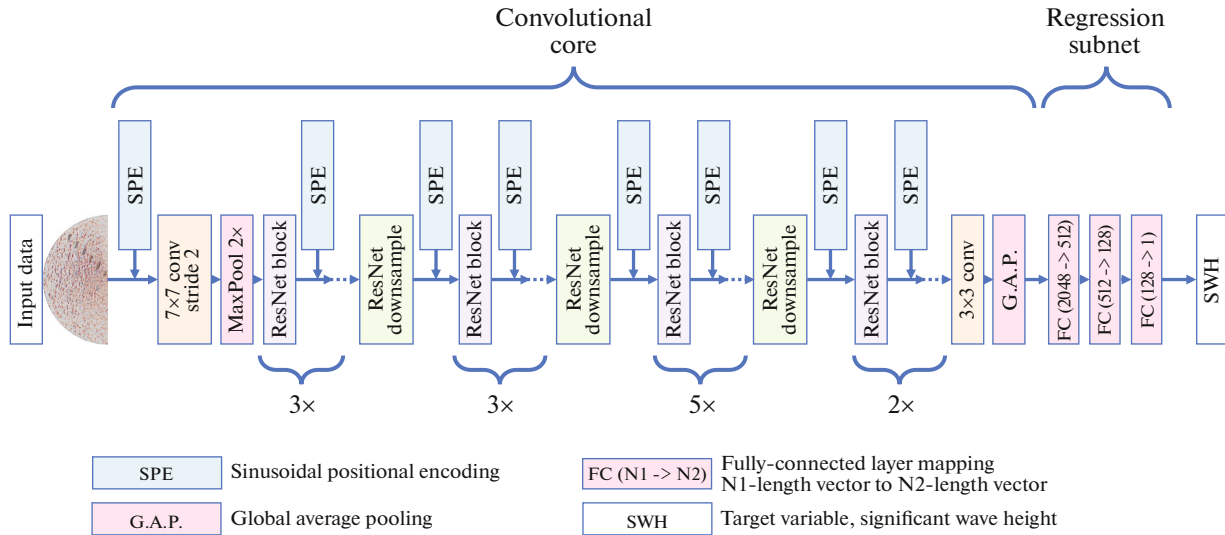
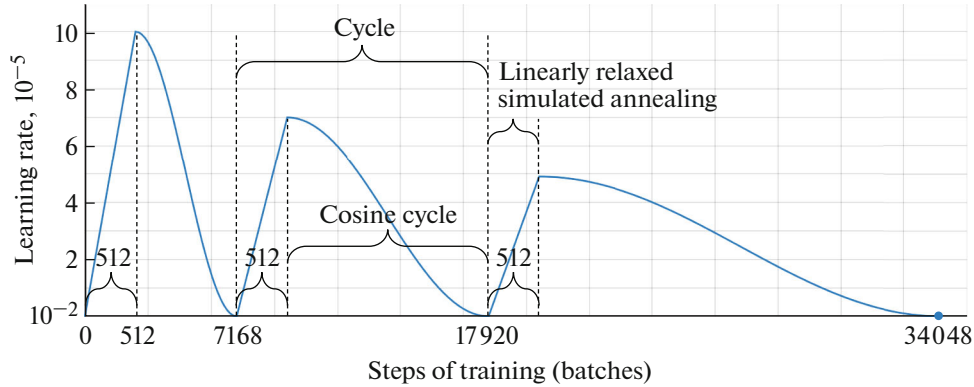**Fig. 5.** High-level architecture of the CNN presented in this study.



**Fig. 6.** Learning rate schedule used while training the CNN in our study.

in SWH regression, but also strong generalization skills. Generalization can be assessed by examining the gap between the quality estimated on the training and testing subsets, with a small gap indicating good generalization and a large gap indicating poor generalization.

In accordance with the latest research, we utilized a specialized learning rate schedule as proposed by Loshchilov and Hutter in 2016 [29]. This cyclical schedule incorporates a cosine-shaped decrease in learning rate over training process along with multiple annealing simulations. Several modifications to this schedule have been proposed in recent studies, and we utilized a configuration that includes the following features:

- We implemented a multiplicative form of increase in the period of simulated annealing with each cosine cycle (see Eq. (1)):

$$T_i = T_0 k_T^{(i-1)}, \qquad (1)$$

where $T_0$ is the number of batches in the first cosine cycle until the first simulated annealing, and $T_0 = 7168$ in our study; $k_T$ is the multiplicative coefficient for the length of cosine cycles, and $k_T = 1.5$ in our study; $i$ is the cycle number starting from $i = 1$.

- We incorporated a linear increase in the learning rate prior to each cycle of cosine-shaped learning rate decay to mitigate sudden changes in gradient moments that can occur within the Adam algorithm.

- We also applied exponential decay of simulated annealing magnitude with each cosine cycle using the multiplicative form (see Eq. (2));

$$A_{sa,i} = A_{sa,0} k_{sa}^{(i-1)}, \qquad (2)$$

where $A_{sa}$ refers to the scale of simulated annealing relative to the initial learning rate, with $A_{sa,0}$ representing its initial value. In our study,
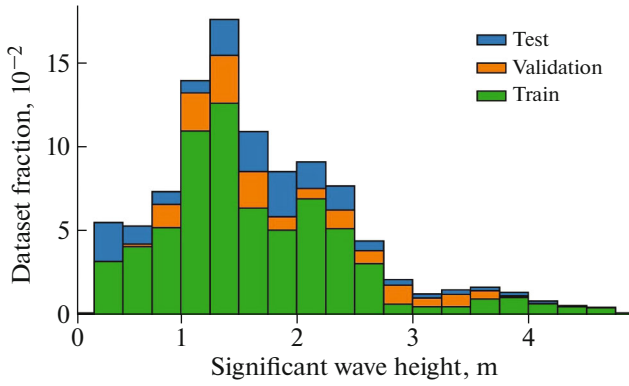
**Fig. 7.** Learning rate schedule used while training the CNN in our study.

$A_{sa,0} = 1$. The multiplicative coefficient $k_{sa}$ was set to 0.8, indicating a decrease in simulated annealing magnitude with each annealing cycle. Finally, $i$ represents the cycle number, starting from $i = 1$.

The resulting learning rate schedule is presented in Fig. 6.

### 3.3. Sampling Strategy for Reliable Quality Assessment

In our study, we assess the quality of our solution for SWH estimation with artificial neural networks in terms of determination coefficient $R^2(\text{SWH}_m, \text{SWH}_{gt})$ and root mean squared error $\text{RMSE}(\text{SWH}_m, \text{SWH}_{gt})$, where $\text{SWH}_m$ is the estimates of SWH with our CNN model, $\text{SWH}_{gt}$ is ground truth SWH values computed using Spotter buoy readings.

In studies exploring the use of statistical models, specifically artificial neural networks, in analyzing remote sensing data to estimate significant wave height, it is important to consider the autocorrelation present in the observational time series dataset. Due to the natural evolution of underlying physical phenomena, successive observations may exhibit strong autocorrelation, which can affect the accuracy of the model.

In machine learning, it is common to evaluate the model's performance by estimating quality metrics on a testing subset acquired through random sampling from the original set of labeled examples. However, this approach assumes that the examples are independent and identically distributed (i.i.d.), which may not hold true for successive SeaVision radar images with strong autocorrelation. Thus, it is crucial to avoid systematically adding successive examples to

the training and testing sets, and instead use methods of sampling specifically designed for time-series data [30−33].

In this study, we address the issue of strongly correlated successive examples by implementing station-wise random sampling, similar to sampling strategy employed in [14−16], which allows for avoiding systematic sampling of successive examples to the training and testing/validation subsets. By doing so, we assess the quality of our model reliably.

Another challenge in statistical modelling is the issue of covariate shift, which refers to a degraded model quality when evaluating it with testing data characterized by a shifted distribution compared to the training subset. To reliably assess model quality, the testing/validation subset of data should follow the same distribution as the training subset.

In our study, we propose a simple sampling strategy to encourage, but not guarantee, matching distributions of data in the training, validation, and testing subsets. Specifically, we employ station-wise sampling stratified with respect to the mean significant wave height (SWH). Figure 7 presents the overall distribution of the target variable (SWH) and an example of the training-validation-testing split in the form of example counts shown by different colors in each bin of the histogram. By using this strategy, we can help ensure that the model is accurately evaluated and trained on data with similar distributions.

To evaluate the effectiveness of our sampling strategy, we utilized seven different train-test splits. We trained the network on the training subset and evaluated the quality metrics on the testing subset for each split. Next, we estimated the mean for each quality metric and assessed their uncertainty $S_m$, where m represents a metric.

To assess $S_m$, we assumed normal distributions for each metric and calculated $S_m$ as a confidence interval with a 95% confidence level based on the sample estimate of the standard deviation computed using the sample of seven train-test splits.

## 4. RESULTS AND DISCUSSION

Using the sampling strategy described in Subsection 3.3 and data preprocessing routine proposed in Subsection 2.1, we trained the CNN presented in Section 3 on the dataset that we collected in our scientific marine cruises (see its summary in Section 2). In this section, we present the results of our approach to estimating SWH from SeaVision radar imagery.

In Fig. 8, we present a scatter diagram demonstrating accordance between SWH values, estimated by our CNN using SeaVision radar imagery, and
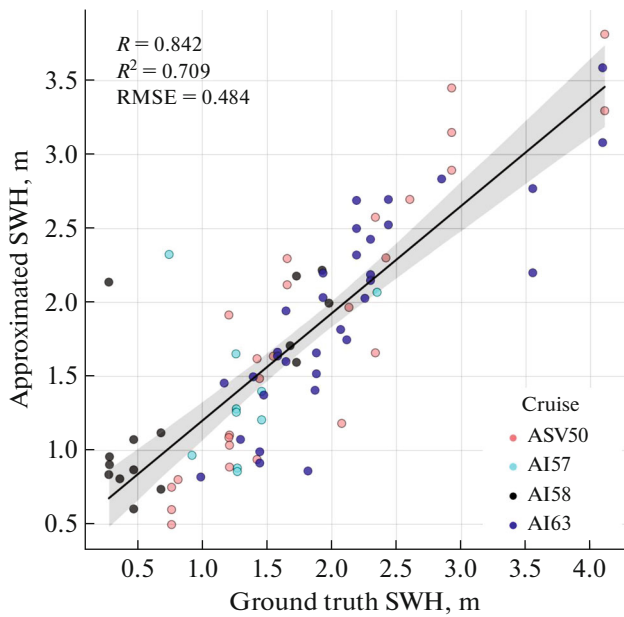
**Fig. 8.** Scatter diagram of approximated SWH in our study.



**Fig. 9.** Error distribution of our CNN. We also show here the kernel density estimate of error distribution with the smooth line on top of the histogram.

ground truth SWH values estimated using Spotter buoy measurements. The data points in the scatter diagram are the points of averaged values from each buoy station accompanied by SeaVision radar imagery. Only hold-out subsets of each train-validation-test split are shown in this scatter diagram. One may clearly see that the correspondence between approximated SWH and ground truth SWH is good, and the uncertainty is not very high. The determination coefficient is $R^2 = 0.71$, which means high correlation $R = 0.84$; and root mean squared error of our CNN-based solution is RMSE = 0.48 m.

In Fig. 8, one may see that there are several outliers in low range of SWH, in particular, one station from AI57 cruise and one station from AI58 cruise. It is worth mentioning that there are known limitations of estimating wind wave characteristics in the case of weak winds (wind speed lower that 3 m/s) or low SWH (SWH lower that 0.5 m). Thus, one may argue that a CNN should be even applied in these cases. We may see, however, that our CNN generally estimates SWH in good accordance with ground truth even in the case of unfavourable (low) wind speeds and significant wave heights.

One may also note a high uncertainty in a high SWH range. We assume that this issue is due to poor data endowment in a high range of target variable SWH. Indeed, from Fig. 7, one may see that the distribution of SWH is skewed towards low SWH values, and there are no events characterized by SWH exceeding 5 m. It is a known issue of monitoring
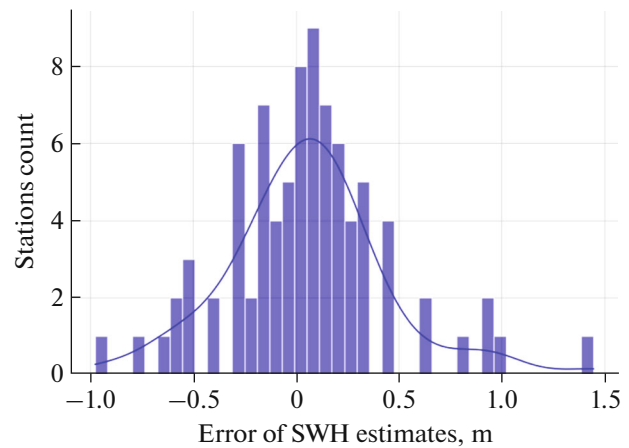
experiments in far seas involving ship-based expeditions. Indeed, the measurements with the Spotter buoy are performed given the ship drifting in order to avoid the influence of both ship-induced waves and ship-enforced migration of the buoy, since these factors both may introduce bias into the estimates of wind wave characteristics. At the same time, keeping a sea vessel adrift preserving it in a controlled state is a difficult task in the case of strong winds or excessive sea waving. Thus, captains commonly do not risk setting our ships adrift in these weather conditions. We plan to extend our dataset of SeaVision imagery accompanied by independent ground truth estimates of sea wave characteristics within alternative setting of the measurement experiment involving underwater acoustic wave gauges or acoustic Doppler current profilers (ADCP) mounted on moorings at the seabed.

In Fig. 9, we present the distribution of errors of CNN-based SWH estimates. The errors are computed in comparison with Spotter buoy ground truth estimates. One may see that the error distribution is zero-centered. Yet one may observe the outliers in the range of high positive errors. Thus, in some rare cases, our CNN overestimates SWH. At the same time, our CNN is not strongly prone to underestimate SWH.

## 5. CONCLUSIONS

In this study, we present a statistical model based on convolutional neural networks (CNN) for estimating wind wave characteristics, in particular, a significant wave height (SWH), from the imagery of X-band marine navigation radar captured and digitized by the SeaVision hardware package. The architecture of our CNN is inspired by ResNet50 with

the modifications of sinusoidal positional encoding, which allows for exploiting periodic structure of wind waves when processing the SeaVision-captured radar imagery of sea clutter. We demonstrate that our approach delivers high-quality estimates characterized by the determination coefficient $R^2 = 0.71$, correlation coefficient $R = 0.84$, and root mean squared error $\mathrm{RMSE} = 0.48$ m, which is close to common quality metrics of classical Fourier-based methods. The need for just one SeaVision radar image in estimating SWH is a strong advantage of the CNN-based approach compared to classical Fourier-based analysis which is characterized by the need of 20 min of radar imagery. One may also note an issue of low data endowment in the range of high SWH values, which has a consequence of suboptimal estimates quality in this range. One may also assume degraded estimation quality in the range of SWH which is not present in the training dataset, meaning that CNN may not exhibit a strong extrapolation ability.

In future work, we are going to extend our dataset to include a larger range of SWH values, particularly in the high range where there is currently poor data endowment. This will make it possible to improve the robustness of our CNN-based approach and ensure that it delivers high-quality estimates across the entire range of SWH values. In addition, we plan to explore the use of pretraining our CNN on synthetic radar imagery of sea clutter to improve the approximation quality. This pretraining will allow the CNN to learn from a larger and more diverse set of data, which should enhance its ability to generalize and extrapolate beyond the range of SWH values present in the training dataset.

Our approach for estimating ocean wave characteristics from shipborne navigation X-band radar data captured by the SeaVision hardware package, which uses artificial neural networks, has the potential to revolutionize global monitoring of ocean waves. Our method is fully automated and computationally inexpensive making it an efficient and cost-effective solution for estimating wave characteristics from radar imagery.

## FUNDING

## CONFLICT OF INTEREST

The authors of this work declare that they have no conflicts of interest.

## REFERENCES

1. J. C. N. Borge, K. Reichert, and J. Dittmer, Coastal Eng. **37**, 331 (1999).
   https://doi.org/10.1016/S0378-3839(99)00032-0
2. R. Gangeskar, in *Proc. IGARSS 2000. IEEE 2000 Int. Geoscience and Remote Sensing Symp., Honolulu, Hawaii, 2000* (IEEE, 2000), Vol. 7, pp. 2952−2959.
   https://doi.org/10.1109/IGARSS.2000.860301
3. C. Greenwood, A. Vogler, J. Morrison, and A. Murray, Remote Sens. Environ. **204**, 439 (2018).
   https://doi.org/10.1016/j.rse.2017.10.012
4. G.-I. Park, J.-W. Choi, Y.-T. Kang, et al., J. Ship Ocean Technol. **10**, 34 (2006).
5. J. Horstmann, J. Bödewadt, R. Carrasco, et al., Sensors **21(23)**, 7828 (2021).
   https://doi.org/10.3390/s21237828
6. N. Tilinina, D. Ivonin, A. Gavrikov, et al., Earth Syst. Sci. Data **14**, 3615 (2022).
   https://doi.org/10.5194/essd-14-3615-2022
7. R. Vicen-Bueno, C. Lido-Muela, and J. C. Nieto-Borge. EURASIP J. Adv. Signal Process. **2012**, 84 (2012).
   https://doi.org/10.1186/1687-6180-2012-84
8. L. Cornejo-Bueno, J. C. Nieto Borge, E. Alexandre, et al., Coastal Eng. **114**, 233 (2016).
   https://doi.org/10.1016/j.coastaleng.2016.04.007
9. N. K. Kumar, R. Savitha, and A. al Mamun, Ocean Eng. **129**, 605 (2017).
   https://doi.org/10.1016/j.oceaneng.2016.10.033
10. J. Mahjoobi and E. Adeli Mosabbeb, Ocean Eng. **36**, 339 (2009).
    https://doi.org/10.1016/j.oceaneng.2009.01.001
11. M. S. Elbisy, J. Coastal Res. **31**, 892 (2015).
    https://doi.org/10.2112/JCOASTRES-D-13-00087.1
12. S. Salcedo-Sanz, J. C. Nieto Borge, L. Carro-Calvo, et al., Ocean Eng. **101**, 244−253 (2015).
    https://doi.org/10.1016/j.oceaneng.2015.04.041
13. M. Krinitskiy, P. Verezemskaya, K. Grashchenkov, et al., Atmosphere, **9**, 426 (2018).
    https://doi.org/10.3390/atmos9110426
14. M. Krinitskiy, M. Aleksandrova, P. Verezemskaya, et al., Remote Sens. **13**, 326 (2021).
    https://doi.org/10.3390/rs13020326
15. M. Krinitskiy, A. Sprygin, S. Elizarov, et al., Remote Sens. **15**, 3493 (2023).
    https://doi.org/10.3390/rs15143493
16. M. Krinitskiy, V. Koshkina, M. Borisov, et al., Remote Sens. **15**, 1720 (2023).
    https://doi.org/10.3390/rs15071720
17. H. Choi, M. Park, G. Son, et al., Ocean Eng. **201**, 107129 (2020).
    https://doi.org/10.1016/j.oceaneng.2020.107129
18. S. Xue, X. Geng, X. H. Yan, et al., J. Oceanogr. **76**, 465 (2020).
    https://doi.org/10.1007/s10872-020-00557-3

19. W. Duan, K. Yang, L. Huang, and X. Ma, Remote Sens. **12**, 1117 (2020).
https://doi.org/10.3390/rs12071117

20. X. Chen and W. Huang, IEEE Trans. Geosci. Remote Sens. **60**, 4201711 (2022).
https://doi.org/10.1109/TGRS.2021.3074075

21. C. C. Wei and H. C. Chang, Sensors **21**, 5234 (2021).
https://doi.org/10.3390/s21155234

22. W. Huang, X. Liu, and E. W. Gill, Remote Sens. **9**, 1261 (2017).
https://doi.org/10.3390/rs9121261

23. A. Gavrikov, D. Ivonin, V. Sharmar, et al., PANGAEA (2021).
https://doi.org/10.1594/PANGAEA.939620

24. K. Raghukumar, G. Chang, F. Spada, et al., J. Atmos. Ocean Technol. **36**, 1127 (2019).
https://doi.org/10.1175/JTECH-D-18-0151.1

25. K. He, X. Zhang, S. Ren, and J. Sun, in *Proc. IEEE Conf. on Computer Vision and Pattern Recognition, Las Vegas, 2016* (IEEE, 2016), pp. 770–778.

26. Z. Li, N. Kovachki, K. Azizzadenesheli, B. Liu, et al., arXiv Preprint (2020).
https://doi.org/10.48550/arXiv.2010.08895

27. R. Liu, J. Lehman, P. Molino, F. Petroski Such, et al., in *Proceedings of the Advances in Neural Information Processing Systems (NeurIPS 2018)*, Vol. 31.

28. D. P. Kingma and J. Ba, arXiv Preprint (2014).
https://doi.org/10.48550/arXiv.1412.6980

29. I. Loshchilov and F. Hutter, arXiv Preprint (2016).
https://doi.org/10.48550/arXiv.1608.03983

30. C. Bergmeir, R. J. Hyndman, B. Koo, Comput. Stat. Data Anal. **120**, 70 (2018).
https://doi.org/10.1016/j.csda.2017.11.003

31. C. Bergmeir, J. M. Benуиtez, Inf. Sci. **191**, 192 (2012).
https://doi.org/10.1016/j.ins.2011.12.028

32. J. Racine, J. Econometrics **99**, 39 (2000).
https://doi.org/10.1016/S0304-4076(00)00030-0

33. S. Arlot, A. Celisse, Stat. Surv. **4**, 40 (2010).
https://doi.org/10.1214/09-SS054

**Publisher's Note.** Allerton Press remains neutral with regard to jurisdictional claims in published maps and institutional affiliations.